J. V. Dave
IBM Corporation
Palo Alto, CA 94304

Effect of Atmospheric Conditions on Remote Sensing of a Surface Nonhomogeneity

The atmospheric blurring effect is a strong function of the amount of haziness in the atmosphere, solar zenith angle, position of the surface feature with respect to the local nadir direction, and wavelength of the radiation.

Introduction

Radiometric sensors on the Landsat, Skylab, and other advanced spacecrafts permit continuous monitoring of the earth-atmosphere system in several spectral regions with a ground-level spatial resolution of 10 to 100 m. Most such monitoring is currently confined to within 8° of the local nadir direction and, as such, a single spacecraft provides data of the same geographic region at about 18 day intervals. Agricultural and several other applications need such remotely sensed observations of the Earth's features at intervals of a couple of days. An increase in the temporal resolution can be provided by expanding the angular range of the scan to about 50° (Schnetzler and Thompson, 1979). Even if the physical edges of a given surface feature such as a field or a pond are sharply defined, the presence of the intervening atmospheric screen results in a blurring of the edges, with the degree of resolution loss depending upon the contrast between the feature and its background, on various atmospheric parameters, and several directional parameters of the illumination and viewing geometry. Such blurring effects are well known in photography where they are commonly referred to as the adjacency effects. They arise in the development of high-contrast scenes.

The relatively high resolution of the Landsat sensors results in many data points for a fairly uniform field of several square kilometres. The atmospheric blurring effects are then clearly evident in many scenes for which the ground-truth information is available. Hence, several investigators (e.g., Cicone *et al.*, 1979) have developed information extraction procedures based on an arbitrary stripping of the edge pixels, and on the assumption that the remaining interior pixels are relatively pure. Semi-empirical procedures for correcting the scene radiances for the background

Abstract: *The effect of atmospheric conditions on remote sensing of a surface nonhomogeneity is examined by studying the variations of the satellite-level radiance as a function of the nadir angle of a scan across the nonhomogeneity. The nonhomogeneity is in the form of a square 5 km on a side and with a Lambert reflectivity of 5 percent, and embedded in a horizontal ground with a Lambert reflectivity of 30 percent. The satellite-level radiances are computed for three different atmospheric models with nil, moderate, and very large number of aerosol particles after taking into consideration all orders of scattering. Results are presented to show a very significant and variable dependence of the contamination of the directly-transmitted ground signal on the position of the nonhomogeneity with respect to the local nadir direction, on the solar zenith angle, and on the wavelength of the radiation measured by the typical Landsat sensors.*

Photogrammetric Engineering and Remote Sensing,
Vol. 46, No. 9, September 1980, pp. 1173-1180.

effects have also been proposed (e.g., Potter, 1977; Ueno *et al.*, 1978). Such correction procedures generally make use of the so-called weighted mean albedo of the background for arriving at a nominal value of the correction factor.

Several investigators have looked into the question of the degree of purity of the interior pixels of a scene viewed along the local nadir direction. Ueno *et al.* (1978) suggest that, for the average atmospheric conditions to which their analysis is confined, background features located at a distance greater than 800 m from a pixel would have very little effect on the purity of the pixel. Their statement is based on geometric considerations only, and takes into account the strong forward scattering nature of aerosol particles located fairly close to the ground. Otterman and Fraser (1979) point out that the purity of a pixel in the scene can be affected in a significant manner by the reflection characteristics of pixels located at a distance of several kilometres, with the magnitude of the effect determined by several factors such as the relative reflectivities of the scene and the background, the average effective height of the scattering layer, the scattering phase function of the atmospheric constituents, and the attenuation characteristics of the atmosphere between the effective scattering layer and the ground. Their findings are based on a single-scattering approximation and, as such, they are only applicable to observations in the red and near-infrared spectral regions taken under conditions of light haziness. Pearce (1977) uses a backward-tracking Monte Carlo procedure for investigations of the atmospheric blurring effect in the presence of different amounts of aerosols, and for different types of surface nonhomogeneities. His computations are confined to the local nadir direction and, as such, there is no real scan across a boundary separating two different types of grounds. Furthermore, he expresses some reservations in intercomparison of results obtained from statistically independent runs. However, his investigation, aimed at the estimation of the contamination of the central-pixel signal of a square surface nonhomogeneity due to the background albedo, clearly supports the aforementioned findings of Otterman and Fraser.

In this paper, we present selected results of our investigation on variations of the satellite-level radiance as a function of the nadir angle of a scan across a surface nonhomogeneity. The nonhomogeneity is in the form of a square with 25 km² area, and with its sides along the east-west (or north-south) directions. The vertical plane containing the satellite and the direction of scan makes an angle of 45° with the vertical plane passing through the sun and the satellite, i.e., the scan is across the diagonal of the square (Figure 1). The Lambert reflectivities of the nonhomogeneity and the background are taken to be 0.05 (e.g., water) and 0.30 (e.g., bright sand), respectively. Results are presented to demonstrate the dependence of the adjacency effect on the atmospheric aerosol content, on the wavelength of the radiation, on the solar zenith angle, and on the position of the nonhomogeneity with respect to the local nadir direction.

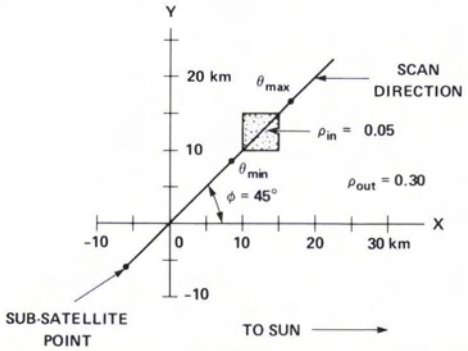

FIG. 1. Schematic of the surface nonhomogeneity, and of the viewing geometry. ϕ is the azimuth angle, the angle between the vertical plane passing through the direction of observation and that passing through the sun and the satellite.

THEORY

Following Chandrasekhar (1950), the radiance, L_g, of the radiation reflected by a uniform Lambert ground of reflectivity, ρ, and illuminated by the direct and diffuse solar radiation transmitted by a plane-parallel atmosphere, is given by

$$L_g = [\rho/(1 - \rho\bar{s})]\cdot f, \tag{1}$$

where $\bar{s}$ is the back-reflectivity of the atmospheric model and f is related to the sum of the direct and diffuse flux of energy incident on the ground. The quantity $\bar{s}$ is a function of several parameters needed in specification of the atmospheric composition, and of the wavelength, λ, of the radiation. The quantity f and hence the radiance, L_g, are functions of all these parameters, as well as of the solar zenith angle, θ_o. The ρ factor appearing in the numerator of Equation 1 is directly responsible for the generation of the L_g term, while that appearing in the denominator represents interactions between the atmosphere and the ground. If the area covered by the surface nonhomogeneity (assumed to exist in the form of an enclosed polygon) is small compared to that of the background, it is permissible to express the radiance of a point inside the nonhomogeneity by the equation

$$L_{g,\text{in}} = [\rho_{\text{in}}/(1 - \rho_{\text{out}}\bar{s})]\cdot f, \tag{2}$$

and that of a point outside the nonhomogeneity by the equation

$$L_{g,\text{out}} = [\rho_{\text{out}}/(1 - \rho_{\text{out}}\bar{s})]\cdot f, \tag{3}$$

where ρ_{in} and ρ_{out} are, respectively, the Lambert reflectivities of the surface representing the nonhomogeneity and the background.

These equations are based on an approximate treatment of the problem of the interaction between a horizontally homogeneous atmospheric model and a nonhomogeneous Lambert ground underneath. The degree of this interaction, as determined from the magnitude of $\bar{s}$, is rather weak. For the extreme case of $\lambda = 0.555$ μm and the atmospheric model with very large amount of aerosols (model:4) for which results are discussed in this paper, $\bar{s}$ is equal to 0.149. Hence, a use of this approximation can result in an over-estimation of $L_{g,in}$ and in an under-estimation of $L_{g,out}$ by a few percent only.

Values of $\bar{s}$ and f for several realistic models of the midlatitude-summer, cloudfree atmosphere are available from our earlier work (Dave, 1978). Position of a point with respect to an enclosed area of any arbitrary shape can be determined by the procedures outlined elsewhere (Dave, 1980). Results are presented in this paper for a square nonhomogeneity, but the method is developed and tested for a polygon of any arbitrary size and shape.

The radiance, L, received at the satellite level in a direction of observation specified by the nadir angle, θ, and the azimuth angle, ϕ, (referred to a vertical plane passing through the sun and the satellite) is the sum of the following three components:

C_1: direct transmission of $L_{g,x}$ (x = in or out) through the atmosphere;

C_2: diffuse transmission of $L_{g,x}$ through the atmosphere; and

C_3: the atmospheric radiation emerging at the top due to illumination of the model from above by the direct solar radiation, and calculated under the assumption that the model is resting on a perfectly absorbing ground.

We then have

$$L = C_1 + C_2 + C_3. \tag{4}$$

The radiance, L, is a function of the parameters needed in the specification of the atmospheric composition, and also of λ, θ_o, θ, ϕ, ρ_{in}, and ρ_{out}.

The C_1 component is given by the equation

$$C_1 = L_{g,x} \exp(-\tau_b/\mu) \tag{5}$$

where $\mu = \cos\theta$ and τ_b is the total normal optical thickness of the model. In the presence of the scattering by aerosols and molecules, as well as that of the absorption by ozone and aerosols, τ_b is given by

$$\tau_b = \tau_b^{(s,R)} + \tau_b^{(s,M)} + \tau_b^{(a,M)} + \tau_b^{(a,Z)} \tag{6}$$

where $\tau_b^{(s,R)}$ and $\tau_b^{(s,M)}$ are the normal scattering optical thicknesses due to scattering by molecules (Rayleigh or molecular scattering) and aerosols (Mie or large particle scattering), respectively, and $\tau_b^{(a,M)}$ and $\tau_b^{(a,Z)}$ are the normal absorption optical thicknesses due to absorption by aerosols and ozone, respectively.

For computing the C_2 component, we first evaluate the primary-scattering source function due to illumination of the atmospheric model from below by a Lambert ground with the specified nonhomogeneity. A procedure for computations of this source function is outlined in the Appendix. After representing this source function with the symbol $J(\tau, \mu, \phi)$ where τ is the total normal optical thickness at a level h km above the ground, we can then compute the primary scattering contribution to C_2 using the following equation:

$$C_{2p} = \frac{1}{\mu} \int_0^{\tau_b} J(\tau,\mu,\phi) \exp(-\tau/\mu)\ d\tau. \tag{7}$$

It may be noted that $J(\tau, \mu, \phi)$ also depends upon the atmospheric composition, and also upon λ, θ_o, ρ_{in}, and ρ_{out}.

As mentioned earlier, values of the quantities $\bar{s}$ and f needed in computations of $L_{g,x}$ are available from our earlier work (Dave, 1978). From this earlier work, we can also obtain values of the C_3 component which takes into account all orders of scattering, and also of the radiance L_{out} emerging at the top of the model when the atmosphere rests on a uniform Lambert ground of reflectivity, ρ_{out}. Using the same procedure and numerical values of various atmospheric parameters in computations of C_{2p} as those used in computations of L_{out} and C_3, we can apply an approximate higher-order scattering correction to the computed values of C_{2p}, and obtain the corresponding values of C_2, provided the values of C_{2p} are computed not only across the nonhomogeneity, but also for several positions away from it where the effects due to the nonhomogeneity are unimportant. Accordingly, we compute values of C_{2p} for a number of values of θ in the angular range $\theta_{min} - \theta_{max}$ shown in Figure 1. The higher-order scattering correction factor, k, at the end points θ_{min} and θ_{max} is then obtained from values of L_{out}, C_1, C_3, and C_{2p} in those two directions by making use of the following:

$$k = (L_{out} - C_1 - C_3)/C_{2p}. \tag{8}$$

Having obtained values of k at the end points, its values for the intermediate values of θ are obtained by a linear interpolation procedure, and values of C_2 are then obtained after multiplying C_{2p} with the corresponding value of k. This is an approximation whose validity cannot be fully established without solving the transfer equation for a three-dimensional model.

From the preceding discussion, it is clear that we have formulated the problem of the radiation transfer for a horizontally homogenous, plane-parallel atmosphere resting on a Lambert ground

containing an arbitrary nonhomogeneity in its surface reflectivity. Furthermore, the higher-order scattering contribution to the emergent radiation arising from the illumination of the atmosphere from below, and interaction between the atmosphere and the ground are accounted for in an approximate manner.

Discussion of Results

General

Results presented in this paper are for scan directions confined to a vertical plane making an angle of 45°, ϕ, with respect to the vertical plane passing through the sun and the satellite. The surface nonhomogeneity is in the form of a square area with a Lambert reflectivity, $\rho_{in} = 0.05$, and embedded in an otherwise uniform Lambert ground with $\rho_{out} = 0.3$ (see Figure 1). The coordinates of the lower left-hand corner of the 5 km sided square nonhomogeneity, referred to the origin, are arbitrarily selected as 10.0, 10.0 km. Values of C_1, C_2, and C_3 are computed for 101 values of θ in the range $|\theta_{min} - \theta_{max}| = 1°$. With a satellite altitude of 600 km above the ground, θ_{min} equals 2°, 22°, and 42° for the sub-satellite point coordinates of (−6, −6), (−163, −163), and (−375, −375) km, respectively.

Computations of the radiance of the beam received at the satellite level are carried out for five different values of the solar zenith angle, θ_o, viz., 0°, 30°, 45°, 60°, and 75°, and for three different atmospheric models with nil, moderate, and very large aerosol contents. These computations are for the wavelengths of 0.555, 0.655, 0.7525, and 0.8675 μm, which are pertinent to the MSS and TM bands of the sensors on Landsat satellites. Out of these, only the 0.555 μm wavelength is in the absorption band of ozone. The remaining three are outside the absorption band of common atmospheric gases. Our atmospheric models contain 0.308 atm-cm of ozone. Information about the vertical profiles of aerosol and ozone used in our computations can be found in Figure 2 of Dave (1978). With the size distribution function *Haze L* plotted in Figure 3 of Dave (1978) and a refractive index of $1.5 - 0.01i$, $\tau_b^{(s,M)} = 0.09109$, and $\tau_b^{(a,M)} = 0.00872$ at $\lambda = 0.555$ μm for model:3 with an average amount of aerosols. The values of $\tau_b^{(s,R)}$ and $\tau_b^{(a,Z)}$ at $\lambda = 0.555$ μm are taken to be 0.09448 and 0.02772, respectively. The aerosol normal optical thicknesses are zero for model:2 with no aerosols. The model with very large amount of aerosols (model:4) contains five times as many aerosol particles as those in model:3 and, hence, its aerosol optical thicknesses are five times those of model:3.

Relative Importance of Various Radiation Components

Values of C_1, C_2, C_3 and $L = C_1 + C_2 + C_3$ are plotted as a function of the nadir angle, θ, in Figures 2, 3, and 4 for the cases of the surface nonhomogeneity contained in the angular range 2°−3°, 22°−23°, and 42°−43°, respectively. These results are for $\lambda = 0.555$ μm and for model:3 with an average amount of aerosols and illuminated by the sun at 60° from the local zenith. These values of the radiances and their components are for the solar irradiance of 172 mW cm^{-2} μm^{-1} (Thekaekara, 1973). The angular size of the nonhomogeneity as seen from the satellite level decreases from about 0.7°, to 0.6°, to about 0.4° with increase in its nadir angular distance from 2.5°, to 22.5°, to 42.5°. The diagonal of the square is about 7 km in length and hence for the closest position of the nonhomogeneity (Figure 2), a 0.1° change in the nadir angle amounts to about a 1 km change in the distance at ground level. In general, for a point inside the square, the most significant contributor to the satellite level radiance is the

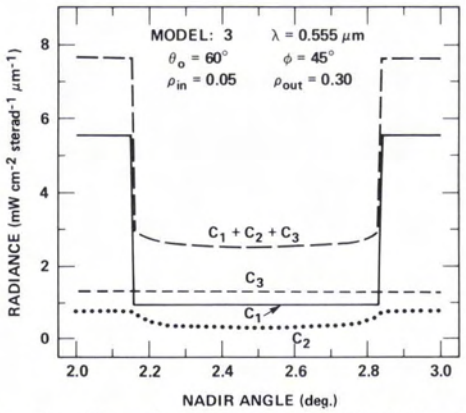

FIG. 2. Directly transmitted (C_1), diffusely transmitted (C_2), and atmospheric (C_3) components of the total ($C_1 + C_2 + C_3$) radiation emerging at the top of the atmospheric model as a function of the nadir angle, θ. Model:3, $\lambda = 0.555$ μm, $\theta_0 = 60°$. θ range: 2°-3°.

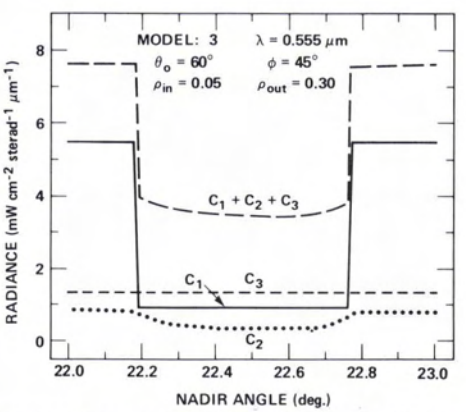

FIG. 3. Same as Figure 2 but for the θ range: 22°-23°.

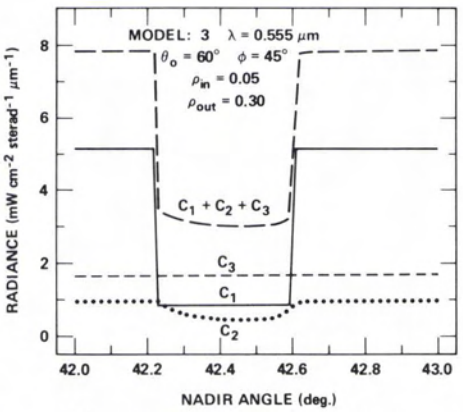

FIG. 4. Same as Figure 2 but for the θ range: 42°-43°.

atmospheric radiation, C_3, whose importance increases with an increase in the distance between the nonhomogeneity and the sub-satellite point. The C_2 component is generally smaller than the C_1 component, but both become comparable near the edges, especially for the farthest position of the nonhomogeneity (Figure 4). The changes in C_2 or $L = C_1 + C_2 + C_3$ with θ near the edge region demonstrate the blurring or the adjacency effect, with the radiation from the bright background spilling over the dark scene. This blurring effect is noticeable to a distance of about 2 km from the edges for the results presented in Figure 2, and all the way to the center for those presented in Figure 4. Furthermore, some asymmetry of the blurring effect can be detected in the results presented in Figure 4. The farther edge is less blurred than the nearer one.

CONTAMINATION OF THE SIGNAL

The directly transmitted component C_1 of the ground-reflected radiation $L_{g,x}$ is diluted by the other two components. It is therefore helpful to work with a contamination factor, η, defined by the equation

$$\eta = (C_1 + C_2 + C_3)/C_1. \tag{9}$$

Variations of the contamination factor, η, as a function of the nadir angle, θ, are plotted in Figures 5 through 7, and Figures 8 through 10 for the cases of the nonhomogeneity confined to the angular range 2°−3° (first or the nearest position) and 42°−43° (third or the farthest), respectively. All these six diagrams are for the 0.555 μm wavelength radiation with each diagram consisting of three curves, one for each of the three atmospheric models described earlier. Figures 5, 6, and 7 (and similarly, Figures 8, 9, and 10) are for solar zenith angles, θ_o, of 30°, 60°, and 75°, respectively. In general, values of the contamination factor outside the nonhomogeneity are smaller than those inside it.

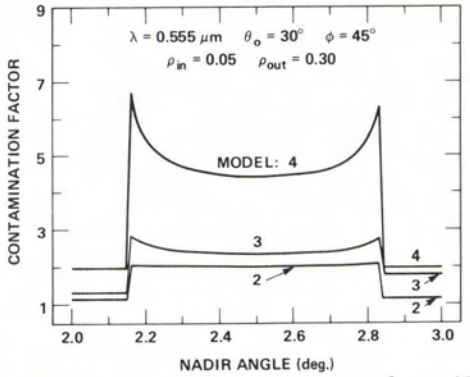

FIG. 5. Variations of the contamination factor $[(C_1 + C_2 + C_3)/C_1]$ as a function of the nadir angle, θ, when the surface nonhomogeneity is confined between $\theta = 2°$ and $\theta = 3°$. Different curves are for atmospheric models with no (model:2), average (model:3), and a very large (model:4) amount of aerosols. $\lambda = 0.555$ μm, $\theta_o = 30°$.

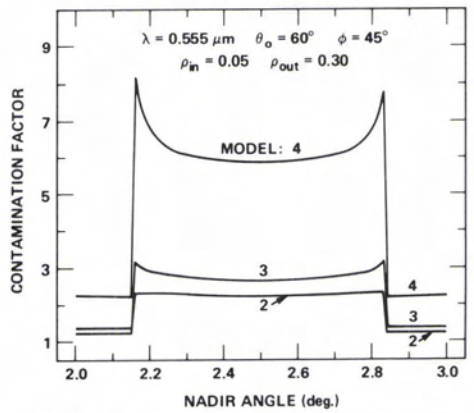

FIG. 6. Same as Figure 5 but for $\theta_o = 60°$.

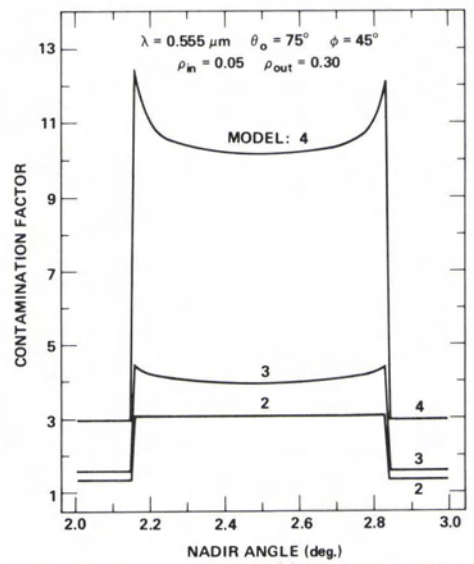

FIG. 7. Same as Figure 5 but for $\theta_o = 75°$.

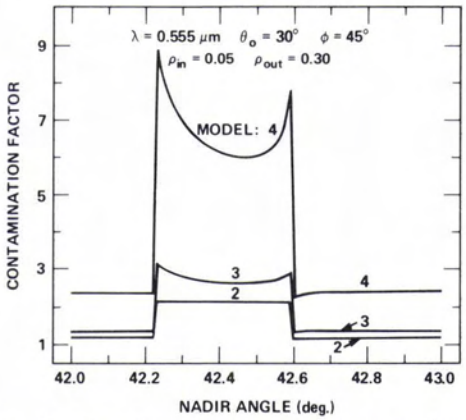

FIG. 8. Variations of the contamination factor $[(C_1 + C_2 + C_3)/C_1]$ as a function of the nadir angle, θ, when the surface nonhomogeneity is confined between $\theta = 42°$ and $\theta = 43°$. Different curves are for different atmospheric models with no (model:2), average (model:3), and very high (model:4) amount of aerosols. $\lambda = 0.555$ μm, $\theta_0 = 30°$.

This is due to the differences in the magnitude of the normalization factor (C_1 in Equation 9) inside and outside the nonhomogeneity.

For model:2 with no aerosols, the contamination factor for the central pixel increases from 2.03 to 3.01 for the first position, and from 2.14 to 3.90 for the third position of the nonhomogeneity as θ_0 is increased from 30° to 75°. However, there is very little edge blurring effect in these cases as it can be visualized from the flatness of the η vs. θ curves within the nonhomogeneity. In all cases, values of the contamination factor increases with an increase in the atmospheric aerosol content with the rate of increase depending upon θ_0 and the angular distance of the nonhomogeneity from the local nadir direction. The blurring, or the adjacency effect, also becomes more pronounced with an increase in these two parameters. For large values of the solar zenith angles and atmospheric aerosol contents, the blurring effect extends to the central pixels of the nonhomogeneity, a distance of about 3.5 km. It is interesting to note that, in such extreme cases, there is a strong asymmetry in the η vs. θ curves within the nonhomogeneity, with the near edge signal more contaminated than the far edge one. Furthermore, the least contaminated pixel is not the central one; it lies somewhere between the central pixel and the far edge pixel (see Figures 8–10).

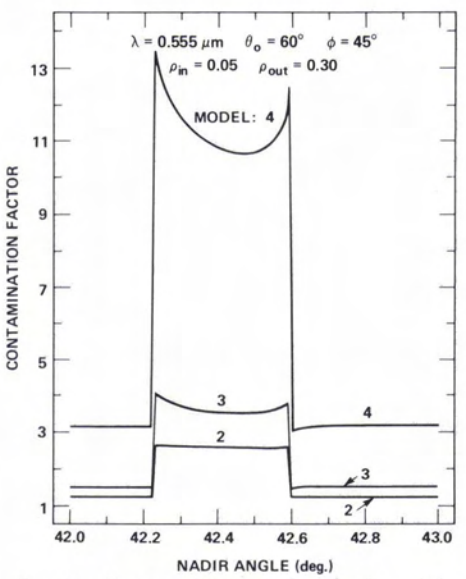

FIG. 9. Same as Figure 8 but for $\theta_0 = 60°$.

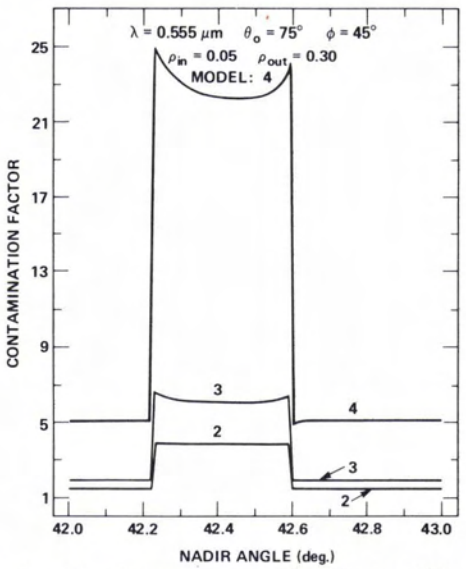

FIG. 10. Same as Figure 8 but for $\theta_0 = 75°$.

Variations of η vs. θ, corresponding to the nearest position (2°–3°) of the nonhomogeneity and for the four wavelengths of interest in Landsat remote sensing, are shown in Figures 11 and 12 for the atmospheric models with average (model:3) and with very large (model:4) amounts of aerosols, respectively. These results are for a solar zenith angle of 60°. From the results presented in these diagrams, it can be seen that the general level of contamination decreases with an increase of the wavelength, but the spread of blurriness over the nonhomogeneity seems to be practically independent of wavelength.

CONCLUSION

In the preceding sections, we have examined numerically the problem of the effects of a high contrast background on the signal received from a small rectangular area (5 km by 5 km) of low reflectivity, and observed through atmospheric

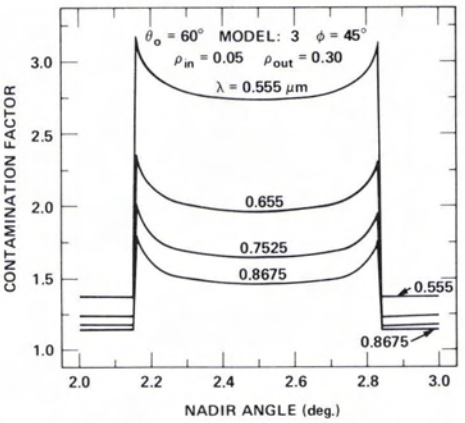

FIG. 11. Variations of the contamination factor $[(C_1 + C_2 + C_3)/C_1]$ as a function of the nadir angle, θ. Different curves are for different wavelengths, λ, of the radiation. $\theta_o = 60°$, model:3 with average amount of aerosols.

models with different amounts of turbidity. For an exact solution of the problem, it is necessary to solve the radiation transport equation for a plane-parallel atmospheric model resting on a horizontally nonhomogeneous ground. A so-called exact numerical solution of this three-dimensional problem is a very formidable task requiring very large computational resources. Hence, an attempt is made to obtain an approximate but meaningful and acceptable solution with the help of the readily available calculations for the one-dimensional models (Dave, 1978). It has been shown that the atmospheric blurring effect is a strong function of the amount of haziness in the atmosphere, solar zenith angle, position of the surface feature with respect to the local nadir direction, and on the wavelength of the radiation. Results of this and other similar investigations can be of considerable assistance in improving of the quality of interpretation of the current and future Landsat data.

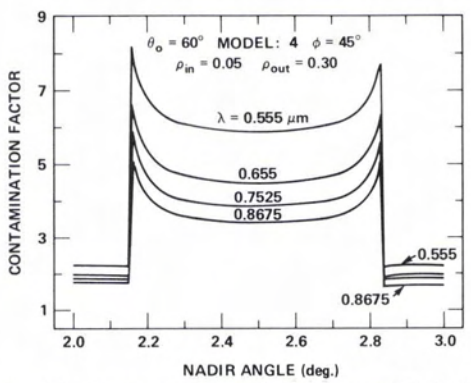

FIG. 12. Same as Figure 11 but for model:4 with very large amount of aerosols.

ACKNOWLEDGMENTS

I would like to take this opportunity to express my sincere thanks to my colleague, Dr. Alan H. Karp, for a reading of the first draft of this manuscript and for his valuable comments, and to Dr. Robert S. Fraser of NASA/Goddard Space Flight Center for bringing to my attention several references of crucial importance to this work.

APPENDIX

PRIMARY-SCATTERING SOURCE FUNCTION DUE TO ILLUMINATION OF THE ATMOSPHERIC MODEL FROM BELOW BY A LAMBERT GROUND WITH A SPECIFIED NONHOMOGENEITY

The source function is defined as the total emission per unit mass in a cone of unit solid angle with its axis along the direction of propagation of the emitted radiation. The direction of emission is represented by the zenith angle, θ (or $\mu = \cos\theta$), and the azimuth angle, ϕ, referred to an arbitrarily chosen vertical plane (see Figure A-1). Integration of this source function weighted by the attenuation factor between the points of emission and reception and the incremental optical thickness along the direction of propagation, provides the radiance of the beam of radiation along the line of sight.

In a non-emitting atmosphere where the rescattering of the atmospheric radiation is neglected, this source function is due to the first scattering of the radiation incident on the atmosphere from outside. The atmospheric optical parameters of interest then are (1) the normalized scattering phase function represented by $P(\tau, \mu, \phi, \mu', \phi')$ where μ' and ϕ' are the directional parameters of the incoming radiation; (2) τ_b is the normal optical thickness of the entire atmosphere; and (3)

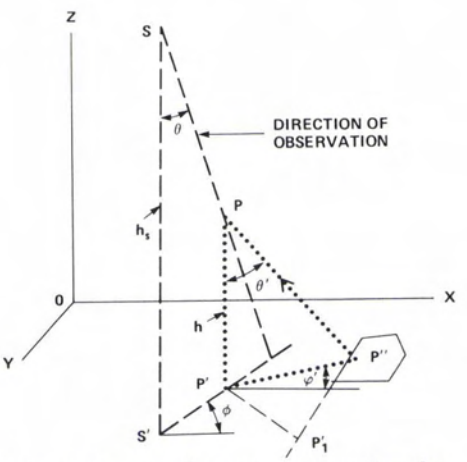

FIG. A-1. Schematic diagram representing the viewing geometry and the ground illumination of a point, P, located on the line of sight.

τ is the normal optical thickness at the point h km above the ground. Further information about these atmospheric optical parameters can be found in several radiation-transfer related publications (e.g., Braslau and Dave, 1973).

Let us consider a plane-parallel atmospheric model of homogeneous character and infinite extent along the horizontal direction, and resting on a horizontal ground obeying Lambert's law of reflection. This ground is assumed to contain a surface nonhomogeneity in the form of an N-sided polygon such that the Lambert reflectivity of the surface inside of the polygon is ρ_{in} and that of outside of the polygon is ρ_{out}.

For the conditions specified in the preceding paragraphs, the expression for the primary-scattering source function is given by

$$\int_0^1 \sum_j \int_{\phi'_j}^{\phi'_{j+1}} \frac{1}{4\pi} P(\tau,\mu,\phi,\mu',\phi')\, L_g(\rho_j,\theta_o) e^{-(\tau_b-\tau)/\mu'} d\mu' d\phi' \qquad (A.1)$$

where L_g (ρ_j, θ_o) is the radiance of the radiation reflected by the Lambert surface of reflectivity, ρ_j. This radiance depends upon the atmospheric composition, surface reflectances, and the solar zenith angle, θ_o.

The factor $\exp[-(\tau_b - \tau)/\mu']$, representing attenuation between the ground and the atmospheric point under consideration, is independent of the azimuth parameter (a consequence of the assumption that the atmosphere is horizontally homogeneous), and hence for integration over ϕ', we deal with the expression

$$\sum_j \int_{\phi'_j}^{\phi'_{j+1}} P(\tau,\mu,\phi,\mu',\phi')\, L_g(\rho_j,\theta_o)\, d\phi'. \qquad (A.2)$$

From the discussion in Dave (1980), it can be shown that, for a given value of μ', the $0-2\pi$ range of ϕ' can be broken up into one or more intervals such that, for the j^{th} interval bounded by ϕ'_j and ϕ'_{j+1}, ρ_j equals either ρ_{in} or ρ_{out}. Thus, for a given $\phi'_j - \phi'_{j+1}$ corresponding to a given value of μ' where L_g (ρ, θ_o) is independent of ϕ', one can obtain a finite integral of the normalized phase function by a suitable numerical quadrature and weigh it with the appropriate value of L_g. The angle, Θ, between the directions (μ, ϕ) and (μ', ϕ') is given by the equation

$$\cos\Theta = \mu\mu' + (1-\mu^2)^{1/2}(1-\mu'^2)^{1/2}\cos(\phi'-\phi), \qquad (A.3)$$

and, hence, a table of $P(\tau, \Theta)$ at 1° interval of Θ would be sufficient for the numerical quadrature in most cases. It should be mentioned that the value of Θ as obtained from Equation A.3 changes from $|\theta - \theta'|$ to $\theta + \theta'$ as ϕ' is increased from 0 to π, and changes from $\theta + \theta'$ to $|\theta - \theta'|$ as $\phi' - \phi$ is increased from π to 2π. It is, therefore, necessary to divide the ϕ' range into a minimum of two intervals (viz., $0 - \pi$ and $\pi - 2\pi$) even if there is no change in the surface reflectivity over the entire range. If ρ_j is not constant over the entire azimuth range of 2π radians, it is necessary to break the ϕ' range at two additional points, viz., ϕ and $\phi + \pi$.

For the integration over μ' appearing in Equation (A.1), a 1° to 2° interval in θ' would be sufficient for most purposes provided θ' is outside the range $\theta'_{min} - \theta'_{max}$. For values of θ' inside this range, an order of magnitude finer resolution may be required, depending upon the physical characteristics of the polygon and desired accuracy of computations.

References

Braslau, N., and J. V. Dave, 1973. Effect of Aerosols on the Transfer of Solar Energy Through Realistic Model Atmospheres. Part I: Non-Absorbing Aerosols, *J. Appl. Met.*, Vol. 12, pp. 601-615.

Chandrasekhar, S., 1950. *Radiative Transfer*, Clarendon Press, Oxford, England.

Cicone, R., E. Crist, R. Kauth, P. Lambeck, W. Malila, and W. Richardson, 1979. *Development of Procedure M for Multicrop Inventory, with Tests of a Spring-Wheat Configuration*, Report No. ERIM 132400-16-F, Contract No. NAS9-15476, Environmental Research Institute of Michigan, Ann Arbor, MI.

Dave, J. V., 1978. Extensive Datasets of the Diffuse Radiation in Realistic Atmospheric Models with Aerosols and Common Absorbing Gases, *Solar Energy*, Vol. 21, pp. 361-369.

————, 1980. *Effect of Atmospheric conditions on Remote Sensing of a Surface Nonhomogeneity*, Report No. G320-3399, IBM corporation Scientific Center, Palo Alto, CA.

Otterman, J., and R. S. Fraser, 1979. Adjacency Effects on Imaging by Surface Reflection and Atmospheric Scattering: Cross Radiance to Zenith, *Applied Optics*, Vol. 18, pp. 2852-2860.

Pearce, W. A., 1977. *A Study of the Effects of the Atmosphere on Thematic Mapper Observations*, Report No. 004-77, Contract No. NAS5-23639, EG&G/Washington Analytical Services Center, Inc., Riverdale, MD.

Potter, J. F., 1977. The Correction of Landsat Data for the Effects of Haze, Sun Angle, and Background Reflectance, *Proceedings, Fourth Annual Symposium on Machine Processing of Remotely Sensed Data*, July 21-23, 1977. IEEE Catalog Number 77CH 1218-7MPRSD, pp. 24-32.

Schnetzler, C. C., and L. L. Thompson, 1979. Multispectral Resource Sampler: An Experimental Satellite Sensor for the mid-1980's, *Proceedings, SPIE Technical Symposium*, May 22-24, 1979, Huntsville, AL.

Thekaekara, M. P., 1973. Solar Energy Outside the Earth's Atmosphere, *Solar Energy*, Vol. 14, pp. 109-127.

Ueno, S., Y. Haba, Y. Kawata, T. Kusaka, and Y. Terashita, 1978. The Atmospheric Blurring Effect on Remotely Sensed Earth Imagery, in *Remote Sensing of Environment: Inversion Methods and Applications*, A. L. Fymat, and V. E. Zuev, Eds., Elsevier, Amsterdam, Netherlands.

(Received 21 January 1980; revised and accepted 26 April 1980)